Clinical Perfusion MRI

Techniques and Applications

Edited by **Peter B. Barker**, **Xavier Golay**, and **Greg Zaharchuk**

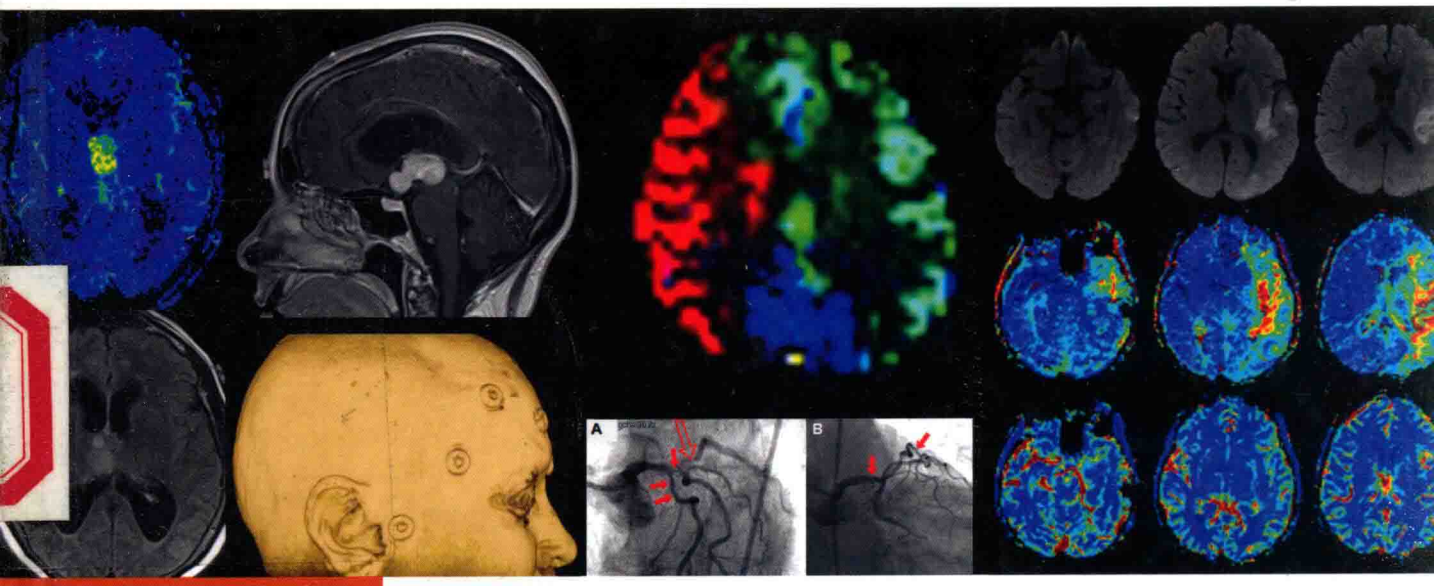

CAMBRIDGE

Medicine

Clinical Perfusion MRI

Techniques and Applications

Edited by

Peter B. Barker DPhil

Professor of Radiology and Oncology, The Russell H. Morgan Department of Radiology and Radiological Science, The Johns Hopkins University School of Medicine, MD, USA

Xavier Golay PhD

Professor and Chair of MR Neurophysics and Translational Neuroscience, Department of Brain Repair and Rehabilitation, UCL Institute of Neurology, University College London, London, UK

Greg Zaharchuk MD, PhD

Associate Professor of Radiology, Stanford University, Stanford, CA, USA

CAMBRIDGE
UNIVERSITY PRESS

CAMBRIDGE UNIVERSITY PRESS
Cambridge, New York, Melbourne, Madrid, Cape Town,
Singapore, São Paulo, Delhi, Mexico City

Cambridge University Press
The Edinburgh Building, Cambridge CB2 8RU, UK

Published in the United States of America by
Cambridge University Press, New York

www.cambridge.org
Information on this title: www.cambridge.org/9781107013391

First published 2013

Printed and bound by Grafos SA, Arte sobre papel, Barcelona,
Spain

A catalog record for this publication is available from the British Library

Library of Congress Cataloging in Publication data

Clinical Perfusion MRI: Techniques and Applications / [edited by]
Peter B. Barker, Xavier Golay, Greg Zaharchuk.
p. ; cm.
Includes bibliographical references and index.
ISBN 978-1-107-01339-1 (Hardback)
I. Barker, Peter B., 1959– II. Golay, Xavier. III. Zaharchuk, Greg.
[DNLM: 1. Magnetic Resonance Angiography–methods.
2. Cerebrovascular Disorders–diagnosis. WN 185]
616.1′307548–dc23
2012039634ISBN 978-1-107-01339-1 Hardback

Clinical Perfusion MRI

Techniques and Applications

PBB To Angela, Blake, Bob, and Ian, gone but not forgotten
XG To Sélène and Lou, for keeping me always on my toes
GZ To Mimi, Kenji, and Noah, with love and appreciation

Contributors

Hongyu An DSc
Biomedical Research Imaging Center and Department of Radiology, University of North Carolina at Chapel Hill, Chapel Hill, NC, USA

Ramon Francisco Barajas Jr. MD
Department of Radiology and Biomedical Imaging, University of California at San Francisco, San Francisco, CA, USA

Peter B. Barker DPhil
Russell H. Morgan Department of Radiology and Radiological Science, Johns Hopkins University School of Medicine, and F. M. Kirby Research Center for Functional Brain Imaging, Kennedy Krieger Institute, Baltimore, MD, USA

David A. Bluemke MD, PhD, MsB, FAHA, FACR
Radiology and Imaging Sciences, Clinical Center, Bethesda, MD, USA

David Bonekamp PhD
Russell H. Morgan Department of Radiology and Radiological Science, Johns Hopkins University School of Medicine, Baltimore, MD, USA

Jonathan Burdette MD
Wake Forest Baptist Health, Department of Radiology, Section of Neuroradiology, Winston-Salem, NC, USA

Soonmee Cha MD
Departments of Radiology and Biomedical Imaging, and Neurological Surgery, University of California at San Francisco, San Francisco, CA, USA

Manus J. Donahue PhD
Departments of Radiology and Radiological Sciences, Neurology, Psychiatry, and Physics and Astronomy, Vanderbilt University School of Medicine, Nashville, TN, USA

Robert R. Edelman MD
Department of Radiology, NorthShore University HealthSystem, Evanston, IL, USA

Riham H. El Khouli MD, PhD
Suez Canal University School of Medicine, Ismailia, Egypt, and Russell H. Morgan Department of Radiology and Radiological Science, Johns Hopkins University, Baltimore, MD, USA

James R. Ewing PhD
Department of Neurology, Henry Ford Hospital, Detroit, MI, USA

Andria D. Ford MD
Department of Neurology, Washington University School of Medicine, Washington University, St. Louis, MO, USA

Xavier Golay PhD
Department of Brain and Rehabilitation, UCL Institute of Neurology, University College London, London, UK

Isky Gordon
ICH – Imaging and Biophysics Unit, Department of Neurosciences & Mental Health, University College London, London, UK

P. Ellen Grant MD
Center for Fetal Neonatal Neuroimaging and Developmental Science, and Departments of Medicine and Radiology, Children's Hospital Boston, Harvard Medical School, Boston, MA, USA

Peter Jezzard PhD
FMRIB Centre, Nuffield Department of Clinical Neurosciences, Oxford University, Oxford, UK

Jin-Moo Lee MD PhD
Departments of Neurology and Radiology,
Washington University School of Medicine,
Washington University,
St. Louis, MO, USA

Weili Lin PhD
Biomedical Research Imaging Center and Department of Radiology,
University of North Carolina at Chapel Hill,
Chapel Hill, NC, USA

Hanzhang Lu PhD
Advanced Imaging Research Center,
University of Texas Southwestern Medical Center,
Dallas, TX, USA

Katarzyna J. Macura MD, PhD
Russell H. Morgan Department of Radiology and Radiological Science,
Johns Hopkins University,
Baltimore, MD, USA

Neel Madan MD
Department of Radiology,
Tufts Medical Center,
Tufts University School of Medicine,
Boston, MA, USA

Joseph A. Maldjian MD
Wake Forest Baptist Health,
Department of Radiology,
Section of Neuroradiology,
Winston-Salem, NC, USA

Blake E. McGehee MD
Wake Forest Baptist Health,
Department of Radiology,
Section of Neuroradiology,
Winston-Salem, NC, USA

James P. B. O'Connor
Centre for Imaging Sciences,
University of Manchester,
Manchester, UK

Geoff J. M. Parker PhD
Centre for Imaging Sciences,
Biomedical Imaging Institute,
University of Manchester, Manchester, UK

Pottumarthi V. Prasad PhD
Department of Radiology,
NorthShore University HealthSystem,
Evanston, IL, USA

Norbert Schuff PhD
Center for Imaging of Neurodegenerative Diseases,
Veterans Affairs Medical Center, and Department of Radiology and Biomedical Imaging,
University of California at San Francisco,
San Francisco, CA, USA

Jürg Schwitter MD
University Hospital Lausanne,
Lausanne, Switzerland

Huan Tan PhD
Department of Radiology,
NorthShore University HealthSystem,
Evanston, IL, USA

Paul S. Tofts PhD
Brighton and Sussex Medical School,
Falmer, Sussex, UK

Jinsoo Uh PhD
Advanced Imaging Research Center,
University of Texas Southwestern Medical Center,
Dallas, TX, USA

Matthias J. P. van Osch PhD
C. J. Gorter Center for High Field MRI,
Department of Radiology,
Leiden University Medical Center,
Leiden, the Netherlands

Katie L. Vo MD
Department of Radiology,
Washington University School of Medicine,
Washington University, St. Louis, MO, USA

Greg Zaharchuk MD, PhD
Radiological Sciences Laboratory, Stanford University, Stanford, CA, USA

Foreword

Diseases of the brain remain the largest single cause of human suffering worldwide [1], and an extraordinarily wide range of symptoms can be observed with brain ischemia, including both acute and chronic neurological and/or psychological deficits. These two facts have prompted a very long quest to better understand, observe, and quantify blood flow in the living human brain – more than a century-long quest, in fact [2]. The advent of in vivo advanced imaging techniques in humans has therefore perhaps naturally been put to use to study blood flow to the brain, and indeed all organs.

While routine imaging of the larger vessels has become relatively straightforward, with a variety of imaging methods ranging from ultrasound to X-rays and beyond to magnetic resonance imaging (MRI), the measurement of tissue-level blood flow has been more challenging. The ability to measure capillary-level blood flow, or tissue perfusion, is of perhaps greater medical importance since the cell is the critical functional entity of human biology. However, methods to measure the various parameters that characterize tissue perfusion have been frankly more challenging than the imaging of the larger vessels in living humans. A variety of methods were initially developed using radioactive tracers, including planar imaging as well as tomographic methods such as positron emission tomography (PET) or single-photon emission computed tomography (SPECT). The fundamental principles of these methods have since been adapted for use with the currently far more widely available modalities of X-ray computed tomography (CT) and MRI.

In 1991, Belliveau and colleagues [3] at the Massachusetts General Hospital demonstrated that brain perfusion could be measured in humans with MRI using bolus injection of MR contrast agent, a technique which has become known as dynamic susceptibility contrast (DSC) MRI. This technique is a use of contrast agents that has regulatory approval in some countries, with more countries actively considering approval at the time of this writing. Initial applications were in the brain, most notably for studying functional brain activation and the evaluation of patients with cerebrovascular disease, and this methodology is now widely used in clinical practice. The related technique of dynamic contrast-enhanced (DCE)-MRI also looks at contrast agent kinetics following bolus injection, but over a slightly slower time scale, and has found application in oncological imaging applications, perhaps most frequently in the clinical evaluation of lesions of the breast. In the early 1990s, landmark papers by Detre *et al.* and Williams *et al.* [4, 5] demonstrated the ability to image cerebral blood flow entirely non-invasively, without the injection of an exogenous tracer, a technique now known as arterial spin labeling (ASL)-MRI. Although the utilization of this method in routine clinical neuroimaging has been somewhat less compared to DSC, perhaps because of some of the technical difficulties (now mostly overcome), the method is beginning to be used with increasing frequency. For all of these methods, the greatest volume of studies to date have been performed in the brain, with applications to other organ systems mostly still at an earlier stage of development.

In 2000, when Peter Reimer and I wrote the book *Cerebral MR Perfusion Imaging: Principles and Current Applications* [6], only DSC was in routine clinical use. Since then, the use of ASL, DCE, and DSC has steadily progressed, both for neuro- and non-neuro imaging applications. The current book covers these more recent advances, and gives the reader an excellent understanding of the theoretical and experimental aspects of perfusion MRI. For the clinician or researcher, in addition to a knowledge of data acquisition methods, it is of particular importance to understand the algorithms and analysis methods used to generate perfusion maps from the raw MR image data. Careful consideration of many factors is required in order to generate reproducible,

quantitative perfusion images. This book not only describes recommended acquisition and analysis procedures, but also discusses limitations and potential pitfalls that may be encountered. While not every clinical case may require quantitative measurement, without a firm grasp of the techniques and their associated strengths and weaknesses, the interpreter will ultimately be limited in their ability to draw conclusions, and hence the need for this book. Case reports at the end of the clinical chapters describe how such methods can be applied in real-life situations.

With the popularity of perfusion MRI and its ability to aid in sorting through clinical questions has come greater support from equipment manufacturers. All major equipment vendors now provide substantial support for clinical perfusion MRI, and the role of microvascular flow continues to be of critical importance, indeed increasingly appreciated importance, in many diseases. One recent example is the advent of anti-angiogenic therapy, where the need to understand tumor- and organ-level microvascular flow has taken on tremendous importance. I expect that many additional areas will emerge as we gain greater insight into human physiology, and I also expect perfusion MRI to continue to develop and mature technically. This book, therefore, is timely and needed, as it provides both clinicians and researchers with a comprehensive and state-of-the-art evaluation of perfusion MRI.

Gregory Sorensen
Chief Executive Officer Siemens Healthcare North America
Boston, Massachusetts
2012

References

1. World Health Organization. *The Global Burden of Disease: 2004 Update*. Geneva: WHO, 2008.
2. Roy CS, Sherrington CS. On the regulation of the blood-supply of the brain. *J Physiol* 1890;**11**:85–108.
3. Belliveau JW, Kennedy DN Jr., McKinstry RC, *et al.* Functional mapping of the human visual cortex by magnetic resonance imaging. *Science* 1991;**254**:716–19.
4. Detre JA, Leigh JS, Williams DS, Koretsky AP. Perfusion imaging. *Magn Reson Med* 1992;**23**:37–45.
5. Williams DS, Detre JA, Leigh JS, Koretsky AP. Magnetic resonance imaging of perfusion using spin inversion of arterial water. *Proc Natl Acad Sci U S A* 1992;**89**:212–16.
6. Sorensen AG, Reimer P. *Cerebral MR Perfusion Imaging: Principles and Current Applications*. New York, NY: Thieme, 2000.

Preface

Blood flow is one of the most fundamental physiological parameters. Maintenance of adequate blood flow is vital for the health of biological tissue. The growth and function of many organ systems are linked tightly to their blood supply. In addition, many disease processes are associated with either increases or decreases in flow compared with normal values. The development and validation of non-invasive tools for the measurement of flow have been longstanding goals, both in biomedical research and in clinical practice.

Traditionally, the imaging of flow, or perfusion, has been accomplished using either nuclear medicine-based techniques involving radioactive isotopes, or X-ray computed tomography (CT) methods using radio-opaque contrast agents. However, soon after the introduction of magnetic resonance imaging (MRI) for anatomical imaging, research began on techniques for depicting flow. Since then, progress has been rapid, not least because MR methods have the advantage of not involving radiation, and in the case of arterial spin labeling-based techniques, are completely non-invasive. This makes them particularly appealing for use in a wide range of populations, including children and normal subjects. In addition, MR perfusion can be combined with the armamentarium of other structural, vascular, physiological, metabolic, and functional techniques available with MR to provide a comprehensive, "one-stop" examination for the patient.

Perfusion MRI is now a part of clinical practice, most notably for evaluating neurological disease. In particular, these techniques have been most developed for studying cerebrovascular disease and tumors of the central nervous system (CNS). However, perfusion MRI also has had a major impact in certain organ systems outside the CNS, including the breast, heart, and prostate. Techniques and applications continue to be developed, and over time perfusion MRI is likely to become widely used in organ systems throughout the body.

This book is divided into two major parts, the first section covering the theoretical background of the measurement of perfusion, technical aspects of dynamic susceptibility contrast (DSC) and dynamic contrast enhancement (DCE), and arterial spin labeling (ASL). Chapters are also included on its use in neuroscience (including functional MRI), and MRI methods for measuring blood volume and oxygenation. The second section contains a comprehensive review of clinical applications of perfusion MRI, in neurological diseases including stroke and brain tumors, neurodegeneration, as well as applications throughout the body (breast, heart, prostate, and other organ systems). Finally, there is a chapter dedicated to perfusion MRI in pediatrics.

This book is mainly focused on perfusion MRI in humans; however, on occasion, reference is made to preclinical studies when appropriate. However, it is not intended to be a reference work for researchers using preclinical MRI in animal models, even if many of the principles and techniques for clinical and preclinical perfusion MRI are similar. Other areas that this book does not specifically cover include vascular imaging (i.e., MR, CT, or X-ray angiography), MR perfusion using unconventional or unapproved tracers, or other non-MR methods of measuring perfusion, such as X-ray CT perfusion (CTP) or positron emission tomography (PET). These topics are beyond the scope of the current volume.

Despite the popularity of perfusion MRI in clinical use, there is currently a need for a book that covers this topic in detail. *Clinical Perfusion MRI: Techniques and Applications* aims to fill this gap, and to provide the reader with a comprehensive, yet readable, treatment of this topic. In a single volume, it provides clinicians with the basic knowledge needed to use this technique in their clinical practice. The widespread adoption of high-quality, clinical perfusion MRI will result in improved diagnoses and management decisions, resulting in better clinical outcomes in individual patients worldwide.

Abbreviations

AAT	arterial arrival time
aBV	arterial blood volume
ACA	anterior cerebral artery
ACE-I	angiotensin-converting enzyme inhibitor
ACS	acute coronary syndrome
ACZ	acetazolamide
AD	Alzheimer's disease
ADC	apparent diffusion coefficient
AIF	arterial input function
AMI	acute myocardial infarction
ASE	asymmetric spin echo
ASL	arterial spin labeling
ASPECTS	Alberta Stroke Program Early CT Score
ATA	arterial transit artifact
ATT	arterial transit time (ms)
AUC	area under the curve (for ROC analysis)
AV	atrioventricular
BAT	bolus arrival time (ms)
BOLD	blood oxygenation level-dependent contrast
BV	blood volume
CA	Contrast agent
CAD	computer-assisted diagnosis; or coronary artery disease
CAS	carotid artery stenting
CBF	cerebral blood flow (ml/100 g/min)
CBV	cerebral blood volume (ml/100 g)
cCBV	corrected cerebral blood volume (usually corrected for leakage of contrast)
CFR	cardiac flow reserve
CHD	congenital heart disease
$CMRO_2$	Cerebral metabolic rate of oxygen consumption (mmol O_2/100 g/min)
CNR	contrast-to-noise ratio
CNS	central nervous system
COMI	cerebral oxygen metabolic index
CPP	cerebral perfusion pressure (mmHg)
CS	coronary sinus
CT	computed tomography
CTA	CT angiography
CTA	Computed tomography angiography
CTC	contrast concentration versus time curve
CTP	CT perfusion
CXA	coronary X-ray angiography
DCE	dynamic contrast enhancement
dHb	deoxyhemoglobin
DMN	Default mode network
DNP	Dynamic nuclear polarization
DSA	digital subtraction angiography
DSC	dynamic susceptibility contrast
DWI	diffusion-weighted imaging
EBCT	electron beam CT
EBRT	external beam radiation therapy
ECG	electrocardiogram
EES	extravascular extracellular space
EPI	echo-planar imaging
EPISTAR	EPI-based signal targeting by alternating radiofrequency pulses, an early pulsed ASL sequence
FA	flip angle
FAIR	flow alternating inversion recovery, one of the early pulsed ASL sequences
fMRI	functional MRI
FSE	fast spin echo
FSL	Functional magnetic resonance imaging of the brain Software Library, a freeware post-processing imaging toolkit from the Univeristy of Oxford
FTD	frontotemporal dementia
FTLD	Frontotemporal lobar degeneration
GABA	gamma-aminobutryic acid, an inhibitory neurotransmitter
GE	gradient echo
GESSE	gradient echo sampling under the spin echo
GFR	glomerular filtration rate
GM	gray matter
GRASE	gradient and spin echo
GRE	gradient echo
HbO_2	oxyhemoglobin
Hct	hematocrit
HHT	hereditary hemorrhagic telangiectasia
HII	hypoxic-ischemic insult
ICA	internal carotid artery
ICDs	implanted cardioverter-defibrillators
ICV	intracranial volume (cm^3)
IVD	ischemic vascular dementia
JPA	juvenile pilocytic astrocytoma
K^{trans}	Forward rate constant for transfer of a contrast agent between the vascular and extravascular space
LGE	late gadolinium enhancement, a marker of dead tissue on cardiac MR
LV	left ventricular
MACE	major adverse cardiac events
MAGIC	multiple acquisitions with global inversion cycling
MCA	middle cerebral artery
MCI	mild cognitive impairment
MDCT	multi-detector CT

MEG	magnetoencephalography
MEGESE	multi-echo gradient echo/spin echo
MION	monocrystalline iron oxide nanoparticles, a type of USPIO
MITR	maximum intensity change per unit time interval ratio
MRA	magnetic resonance angiogram
mRS	modified Rankin score
MRS	magnetic resonance spectroscopy
MRV	magnetic resonance venography
MT	magnetization transfer
MTT	mean transit time (in seconds)
NAC	neo adjuvant chemotherapy
NASCET	North American Symptomatic Carotid Endarterectomy Trial, from which a standard grading system for arterial stenosis has been derived
NPV	negative predictive value
NSF	nephrogenic systemic fibrosis
PASL	pulsed arterial spin labeling
PC	phase contrast
PCA	posterior cerebral artery
pCASL	pseudo-continuous ASL, sometimes also called pulsed-continuous ASL
PCI	percutaneous coronary intervention (angioplasty and stent placement)
pCT	perfusion CT
PE	pulmonary embolism
PET	positron emission tomography
PFS	progression-free survival
PH	peak height
PICORE	Proximal inversion with a control for off-resonance effect
PK	pharmacokinetic
PLD	post-label delay (in seconds), used primarily for continuous or pseudo-continuous ASL sequences
PNET	primitive neuroectodermal tumor
PPV	positive predictive value
PS	permeability surface area product
PSR	percentage of signal recovery (in bolus DSC)
PVL	periventricular leukomalacia
PWI	perfusion-weighted imaging
Q2TIPS	Second version of quantitative imaging of perfusion by using single subtraction with addition of thin-section periodic saturation after inversion and time delay
qBOLD	quantitative blood oxygenation level-dependent contrast
QSM	quantitative susceptibility mapping
QUASAR	Quantitative signal targeting by alternating radiofrequency labeling of arterial regions, a multi-delay ASL sequence
QUIPSS I	Quantitative Imaging of Perfusion using a Single Subtraction method I
QUIPSS II	Quantitative Imaging of Perfusion using a Single Subtraction method II
QUIXOTIC	QUantitative Imaging of Extraction of Oxygen and Tissue Consumption
$R(t)$	Residue function, or fraction of tracer remaining in the voxel following an infinitely sharp bolus
R_2	$=1/T_2$, Relaxivity rate for spin echo experiments
$R_2^*=1/T_2^*$	R_2^*, Relaxivity rate for gradient echo experiments
RAS	renal artery stenosis
RCC	renal cell carcinoma
RECIST	Response Evaluation Criteria in Solid Tumors
ROC	receiver operator characteristic
ROI	region of interest
rs-fMRI	resting state functional MRI
RVD	renovascular disease
SAGE	Spin and gradient echo
SAR	specific absorption rate
SE	spin echo
SI	signal intensity
SNR	signal-to-noise ratio
SPECT	single photon emission computed tomography
SPM	Statistical Parameter Mapping, a freeware software program that runs within Matlab, from the University College of London
SSFP	steady-state free precession, a method of image readout
STEMI	ST-segment elevation myocardial infarction
SVD	singular value decomposition, a popular method of performing deconvolution
SWI	susceptibility-weighted imaging
TDL	tumefactive demyelinating lesion
TE	echo time
TEE	transesophageal echocardiogram
THM	tissue homogeneity model
TI	inversion time or delay (in pulsed ASL)
T_{max}	normalized bolus delay (in seconds)
TR	repetition time
TRUST	T_2 relaxation under spin tagging
TTE	transthoracic echocardiogram
USPIO	ultrasmall superparamagnetic iron oxide
V/Q scan	ventilation perfusion scan, used in the lung to diagnose pulmonary emboli
VASO	vascular space occupancy
vCBV	venous CBV
VEGF	vascular endothelial growth factor
Venc	velocity-encoding level, used for phase contrast angiography
VOF	venous output function
VS-ASL	velocity-selective ASL
WHO	World Health Organization, a grading system for brain tumors
WM	White matter
WML	White matter lesions
Xe-CT	Xenon-enhanced CT
Y_v	tissue oxygen saturation (%)

Contents

Chapter 1

Imaging of flow: basic principles

James R. Ewing, David Bonekamp, and Peter B. Barker

Key points

- Indicator dilution techniques for measuring blood flow have existed for more than 100 years.
- Indicators may be either intravascular, or freely diffusible.
- Early techniques establishing the mathematical framework for flow (the Fick principle, Kety–Schmidt method, and central volume principle) were mainly based on arterial and venous blood sampling.
- Tissue perfusion measured by MR techniques may be either based on bolus contrast agent injection, or non-invasive, endogenous "magnetic" labeling of inflowing blood.
- MR perfusion is one of a variety of techniques now available for tomographic imaging of flow; competing techniques such as SPECT, PET, and CT are also able to produce perfusion images.

Introduction

The flow of blood to an organ is a fundamental physiological factor affecting tissue health, growth, and repair. Blood flow and volume are perturbed in many disease conditions, most notably in vascular disease and in tumors. The ability to determine non-invasively blood flow and blood volume using imaging methods therefore has important diagnostic and therapeutic implications. Since the early days of radiological imaging, scientists and physicians have been searching for methods that can accurately and non-invasively depict the major blood vessels of the body, and measure blood flow in tissue. For instance, X-ray projection imaging of blood vessels (angiography) was first demonstrated in 1927 by Moniz [1], using iodinated contrast agents injected intravascularly, while early measurements of tissue blood flow were based on the inhalation of freely diffusible tracers (e.g., nitrous oxide [N_2O] [2], or radioactive xenon or krypton [3]). Subsequently, stable (i.e., non-radioactive) xenon was used in conjunction with X-ray computed tomography (CT) to image cerebral blood flow (CBF) [4], while other methods such as single-photon emission CT (SPECT) [5, 6] and positron emission tomography (PET) [7, 8] imaging using a variety of radiotracers also became available. More recently, dynamic CT perfusion imaging using bolus injection of iodinated contrast agents has been growing in popularity [9], particularly as fast multi-slice CT scanners have become widely available.

With the emergence of magnetic resonance imaging (MRI) as a clinical imaging modality in the 1980s and 1990s, MRI methods were developed for both angiography and perfusion. Perfusion imaging methods based on exogenous contrast media [10, 11] as well as completely non-invasive methods based on "magnetic labeling" of inflowing blood [12, 13] were developed. Compared to radioactivity- or X-ray-based perfusion methods, MR perfusion offers the advantage of the absence of radiation (particularly important for patients sensitive to radiation, such as children) as well as a synergistic combination with other MRI techniques that offer exquisite soft tissue contrast and spatial resolution. Today, MR perfusion imaging is increasingly being used in clinical practice. However, accurate quantitative perfusion imaging using MRI also involves many technical challenges.

This chapter describes methods for measuring blood flow, looks back at the history of such

Clinical Perfusion MRI: Techniques and Applications, ed. Peter B. Barker, Xavier Golay, and Greg Zaharchuk. Published by Cambridge University Press.

measurements, and presents the central concepts for flow measurements with their corresponding mathematical expressions. Indicator dilution techniques are the main focus, and will be discussed mainly in the context of perfusion in the brain, but with the understanding that such techniques can often be applied to other organ systems. While this chapter will briefly consider measures of bulk flow in large vessels, it will principally focus on measures of perfusion, i.e., measures of flow that estimate the delivery of blood to the microvessels of an organ.

The Fick principle

Modern measurements of vascular physiology began with Adolf E. Fick's description of a method based on the conservation of mass [14]. The heart-lung system has a single flow input, the vena cava, and a single output, the aorta. The difference in oxygen concentration in arterial and venous blood, $c_a - c_v$, is the change of oxygen concentration in the blood as a result of oxygen consumption by the body's metabolism. If we assume that the rates of cardiac flow (F_c – the cardiac output or "minute volume") and oxygen consumption are constant, then $F_c(c_a - c_v)$ is the amount of oxygen per unit time consumed by the body. Mass balance requires that the quantity per unit time of oxygen exiting the heart-lung system via the aorta equals the amount that came in *via* venous blood, plus the amount of oxygen added during blood passage through the lungs:

$$F_c c_a = F_c c_v + VO_2 \tag{1.1}$$

where VO_2 is the rate of oxygen extraction from the lungs. Thus, cardiac output can be calculated as:

$$F_c = \frac{VO_2}{c_a - c_v} \tag{1.2}$$

The Fick principle, relying as it does on mass balance in flow, provides a robust and remarkably simple basis for an important physiological measurement, cardiac output. However, it is invasive in that it requires arterial and venous blood sampling, and the measurement of VO_2 requires that a closed-circuit breathing apparatus be constructed, with provision for in-line carbon dioxide capture, and a means of replacing the oxygen consumed by the patient. While the Fick principle's clinical significance as a means of measuring cardiac output has declined, its underlying principle – mass balance in flow – remains the theoretical basis for nearly every method of flow measurement.

The central volume principle

The central volume principle was first stated by Stewart [15] as a corollary of the Fick principle, and reiterated by Hamilton *et al.* [16]. Using a linear systems approach, Meier and Zierler [17] generated a closely reasoned presentation of this principle. That paper and subsequent elaborations [18, 19] remain the most elegant and easily understood presentations of indicator dilution theory.

Figure 1.1, similar to that in Meier and Zierler's article [17], represents all the paths that a particle of indicator might take in a vascular system (with volume V) from point A to B. It is assumed that the system is stationary or time-invariant, i.e., that flow rates and paths do not change with time, and that the system has a single input and output. The separate pathways show additive behavior in this linear system, and the system can be decomposed into a sum of smaller and smaller components with single inputs and outputs, until only single capillaries remain. In linear systems terminology, the microvasculature is a "passive reciprocal linear two-port network" [20]. It is reciprocal because the same behavior of the system would be observed if the input and output (points A and B in Figure 1.1) were reversed. It is also assumed that all possible pathways are in-line with the supplying and draining vessels. The indicator injected at point A can be freely diffusible, entirely intravascular, or confined to the vasculature plus specific tissue compartments. The only restriction is that the indicator not be trapped in the system, which is equivalent to the absence of pools in the system (which would equal unaccounted losses of mass flow). Note, however, that the nature of the indicator does affect the inference drawn about the volume of the system.

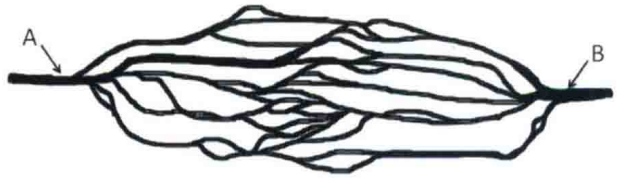

Figure 1.1 A schematic illustration of the paths of the particles of a flow indicator in a vascular system with a single input (A) and output (B). For a freely diffusible indicator, these paths do not necessarily correspond to the paths taken by blood.

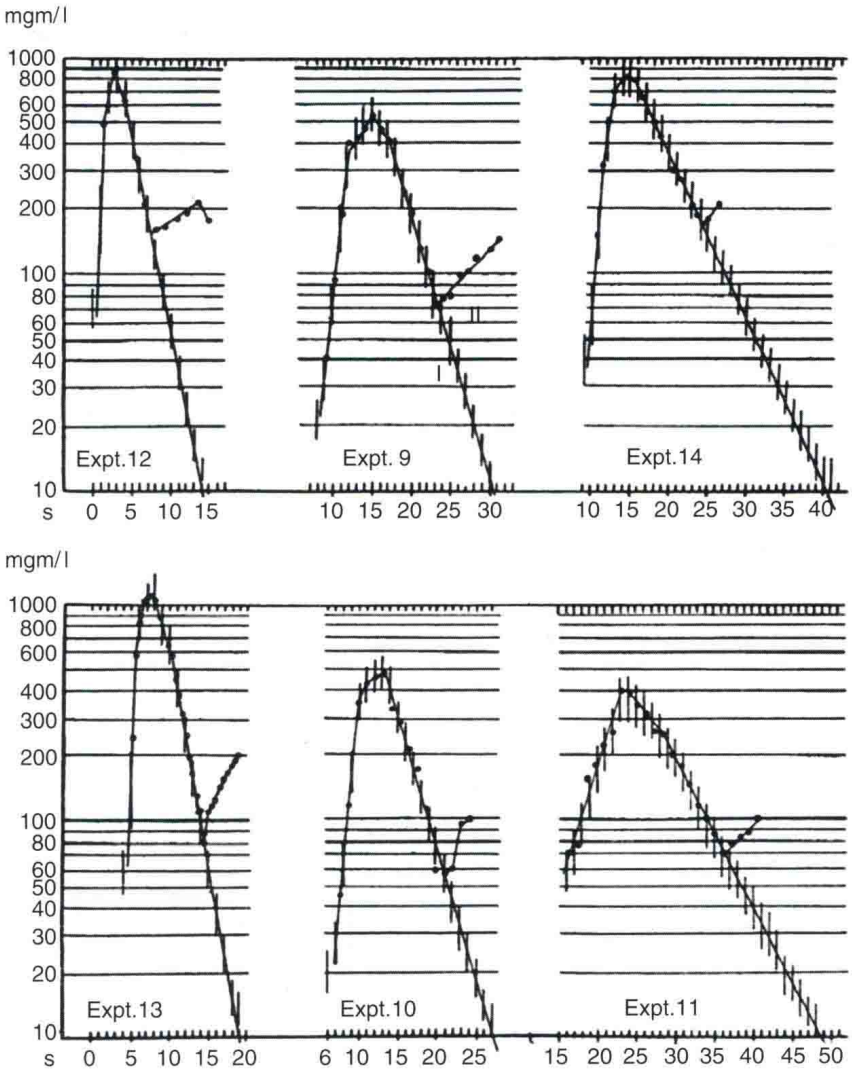

Figure 1.2 Concentration of phenolphthalein dye sampled at various points in the arterial tree of a dog after a bolus venous injection (left ventricle, expts 9, 10, 11, 13; right ventricle, expt. 12; and femoral artery, expt. 14). The log-linearity of a portion of each of the clearance curves is evident. There was very good agreement between estimates of cardiac blood flow made by this method and estimates made by the Fick procedure [21].

If a quantity Q of indicator is injected at point A as an ideal bolus (i.e., a Dirac "delta function") at time $t = 0$, there will be a time lag before the first appearance of the indicator at the exit of the flow system (point B), followed by a rapid rise to a peak concentration, and a more gradual clearance. Figure 1.2, taken from experiments conducted in dogs by Moore *et al.* [21], shows examples of such data, with the concentration of an easily detectable dye (phenolphthalein) sampled at various points in an arterial tree. Note the semi-logarithmic scale of the ordinate in those plots, and the log-linearity of the terminal portion of each clearance curve, indicating that the tracer concentration is decreasing exponentially with time, a sign of a "well-mixed" flow system. The logarithmic slope of the clearance in a well-mixed system should be proportional to the system's flow divided by its volume. The early use of dyes such as phenolphthalein in flow experiments generated the label of "dye dilution," or "indicator dilution" for experiments that utilized a substance that could be assumed not to be metabolized or otherwise trapped in the system.

To derive the central volume principle, consider $Q(t)$, the quantity of tracer that has left the system at point B at time t. The instantaneous quantity of the tracer $(dQ(t)/dt)$ leaving the system at point B during the time interval dt equals the (assumed constant) flow F times the instantaneous concentration $c_B(t)$ at point B times dt: $dQ(t) = F \times c_B(t) \times dt$. Thus, if Q is the total amount of tracer injected,

$$\int_0^\infty \frac{d}{dt} Q(t)dt = Q \tag{1.3}$$

and thus

$$Q = F\int_0^\infty c_B(t)dt \tag{1.4}$$

If tracer quantities and concentrations can be measured directly, this leads to the calculation of the flow according to

$$F = \frac{Q}{\int_0^\infty c_B(t)dt} \tag{1.5}$$

The *transport function*, or the frequency function of transit times, $h(t)$, is defined as follows

$$h(t) = \frac{Fc_B(t)}{Q} \tag{1.6}$$

This quantity has units of inverse time (e.g., 1/min or 1/s). These units result because the product $h(t)dt$ – a unitless quantity – represents an infinitesimal (or instantaneous) probability that a particle of indicator injected at point A at time $t = 0$ will appear at point B at time t. The product $h(t)dt$ therefore is the probability density function (i.e., normalized distribution) of transit times. The ratio on the right-hand side of Eq. (1.6) expresses the amount of tracer passing through point B at the instant t as a fraction of the total injected amount Q.

Therefore $\int_0^\infty h(t)dt = 1$.

To continue with the analogy to probability theory, the cumulative density function (or cumulative distribution function, $H(t)$) and the residue function $R(t)$ are defined:

$$H(t) = \int_0^t h(\tau)d\tau \tag{1.7}$$

$$R(t) = 1 - H(t) \tag{1.8}$$

$H(t)$ is the proportion of indicator particles that have traversed the system from A to B from time 0 to time t, and $R(t)$ is the proportion that remain in the system. Clearly, since all the fluid that enters the system must eventually leave, $H(t) \rightarrow 1.0$ as $t \rightarrow \infty$.

Note that the major difference between classical indicator dilution experiments and modern imaging-based perfusion techniques is the sampling location (see below, External monitoring of indicator concentration). After a bolus input in classical indicator dilution experiments, with sampling performed at point B, the common output vessel of the system, the recorded concentration over the time course of the experiment is a scaled version of the transport function $h(t)$. In imaging experiments, the concentration of indicator in the tissue under observation (voxel) measured over time is a scaled version of the tissue residue function $R(t)$.

The flow rate at which the subset of fluid with transit time t leaves the system is $Fh(t)dt$, where F is the flow in unit volume per unit time. The volume of fluid contained in all microvascular pathways with common transit time τ therefore is $\tau Fh(\tau)d\tau$. To calculate the total volume occupied by tracer (i.e., the distribution volume) between points A and B, we can sum all these separate microvascular pathways, by integrating over all possible values of τ, assuming constant flow (F):

$$V = F\int_0^\infty \tau h(\tau)d\tau \tag{1.9}$$

Remembering that $\int_0^\infty h(t)dt = 1$, it follows from the second mean value theorem for integration that the mean transit time for all indicator (and therefore fluid) particles in the system is expressed as the $h(t)$-weighted average of transit times:

$$\bar{t} = \int_0^\infty th(t)dt \tag{1.10}$$

The combination of Eqs. (1.9) and (1.10), then, yields the *central volume theorem*:

$$V = F\bar{t} \tag{1.11}$$

where $\bar{t}$ is the mean transit time between point A and point B for an indicator particle, and V is the volume of the system accessible to the indicator between point A and point B.

Note that the residue function $R(t)$ has a special relation to the mean transit time since $R(t) = 1 - H(t)$. We can integrate by parts to demonstrate that:

$$\int_0^\infty R(t)dt = \int_0^\infty [1 - H(t)]dt = \{[1 - H(t)]t\}_0^\infty + \int_0^\infty th(t)dt = \int_0^\infty th(t)dt = \bar{t} \tag{1.12}$$